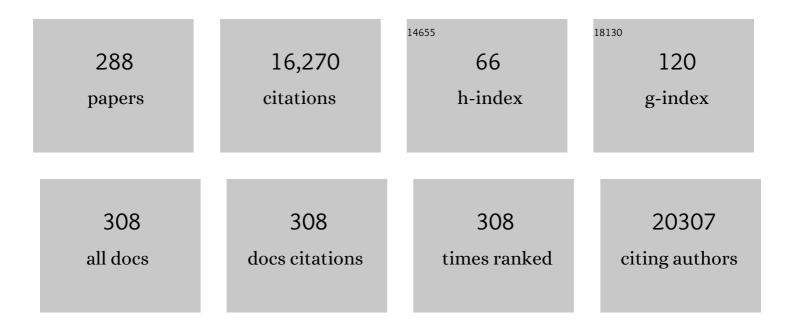
Nigel D Browning

List of Publications by Year in descending order

Source: https://exaly.com/author-pdf/7415863/publications.pdf Version: 2024-02-01



#	Article	IF	CITATIONS
1	Comet 81P/Wild 2 Under a Microscope. Science, 2006, 314, 1711-1716.	12.6	848
2	Formation of the Spinel Phase in the Layered Composite Cathode Used in Li-Ion Batteries. ACS Nano, 2013, 7, 760-767.	14.6	772
3	High Energy Density Lithium–Sulfur Batteries: Challenges of Thick Sulfur Cathodes. Advanced Energy Materials, 2015, 5, 1402290.	19.5	483
4	Direct <i>in Situ</i> Determination of the Mechanisms Controlling Nanoparticle Nucleation and Growth. ACS Nano, 2012, 6, 8599-8610.	14.6	378
5	Controlled Growth of Nanoparticles from Solution with In Situ Liquid Transmission Electron Microscopy. Nano Letters, 2011, 11, 2809-2813.	9.1	332
6	Structural and Chemical Evolution of Li- and Mn-Rich Layered Cathode Material. Chemistry of Materials, 2015, 27, 1381-1390.	6.7	311
7	Investigation of the Mechanism of Mg Insertion in Birnessite in Nonaqueous and Aqueous Rechargeable Mg-Ion Batteries. Chemistry of Materials, 2016, 28, 534-542.	6.7	287
8	Bottom-up construction of a superstructure in a porous uranium-organic crystal. Science, 2017, 356, 624-627.	12.6	286
9	Imaging of Transient Structures Using Nanosecond in Situ TEM. Science, 2008, 321, 1472-1475.	12.6	281
10	Probing the Failure Mechanism of SnO ₂ Nanowires for Sodium-Ion Batteries. Nano Letters, 2013, 13, 5203-5211.	9.1	270
11	Demonstration of an Electrochemical Liquid Cell for Operando Transmission Electron Microscopy Observation of the Lithiation/Delithiation Behavior of Si Nanowire Battery Anodes. Nano Letters, 2013, 13, 6106-6112.	9.1	265
12	A Singleâ€Site Platinum CO Oxidation Catalyst in Zeolite KLTL: Microscopic and Spectroscopic Determination of the Locations of the Platinum Atoms. Angewandte Chemie - International Edition, 2014, 53, 8904-8907.	13.8	263
13	Synthesis of phase-pure and monodisperse iron oxide nanoparticles by thermal decomposition. Nanoscale, 2015, 7, 11142-11154.	5.6	252
14	Photocatalytic Water Oxidation with Nonsensitized IrO ₂ Nanocrystals under Visible and UV Light. Journal of the American Chemical Society, 2011, 133, 7264-7267.	13.7	239
15	Nanoscale Strontium Titanate Photocatalysts for Overall Water Splitting. ACS Nano, 2012, 6, 7420-7426.	14.6	236
16	Conflicting Roles of Nickel in Controlling Cathode Performance in Lithium Ion Batteries. Nano Letters, 2012, 12, 5186-5191.	9.1	231
17	Segregation Effects at Grain Boundaries in Fluorite-Structured Ceramics. Journal of the American Ceramic Society, 2002, 85, 2359-2363.	3.8	219
18	Growth Mechanisms and Oxidation Resistance of Gold-Coated Iron Nanoparticles. Chemistry of Materials, 2005, 17, 3181-3186.	6.7	212

#	Article	IF	CITATIONS
19	Photocatalytic water oxidation with suspended alpha-Fe2O3 particles-effects of nanoscaling. Energy and Environmental Science, 2011, 4, 4270.	30.8	209
20	Observing the Growth of Metal–Organic Frameworks by <i>in Situ</i> Liquid Cell Transmission Electron Microscopy. Journal of the American Chemical Society, 2015, 137, 7322-7328.	13.7	207
21	Comparison of Comet 81P/Wild 2 Dust with Interplanetary Dust from Comets. Science, 2008, 319, 447-450.	12.6	199
22	Overall photocatalytic water splitting with NiOx–SrTiO3 – a revised mechanism. Energy and Environmental Science, 2012, 5, 9543.	30.8	199
23	Nonstoichiometry and the Electrical Activity of Grain Boundaries inSrTiO3. Physical Review Letters, 2001, 86, 4056-4059.	7.8	176
24	Experimental procedures to mitigate electron beam induced artifacts during in situ fluid imaging of nanomaterials. Ultramicroscopy, 2013, 127, 53-63.	1.9	176
25	Nanoscale Phase Separation, Cation Ordering, and Surface Chemistry in Pristine Li _{1.2} Ni _{0.2} Mn _{0.6} O ₂ for Li-Ion Batteries. Chemistry of Materials, 2013, 25, 2319-2326.	6.7	173
26	Direct imaging of single metal atoms and clusters in the pores of dealuminated HY zeolite. Nature Nanotechnology, 2010, 5, 506-510.	31.5	172
27	Direct visualization of initial SEI morphology and growth kinetics during lithium deposition by in situ electrochemical transmission electron microscopy. Chemical Communications, 2014, 50, 2104.	4.1	172
28	Direct Observation of Aggregative Nanoparticle Growth: Kinetic Modeling of the Size Distribution and Growth Rate. Nano Letters, 2014, 14, 373-378.	9.1	172
29	Imaging Isolated Gold Atom Catalytic Sites in Zeolite NaY. Angewandte Chemie - International Edition, 2012, 51, 5842-5846.	13.8	163
30	Evolution of Physical and Photocatalytic Properties in the Layered Titanates A ₂ Ti ₄ O ₉ (A = K, H) and in Nanosheets Derived by Chemical Exfoliation. Chemistry of Materials, 2010, 22, 1220-1228.	6.7	160
31	Single-Crystal Tungsten Oxide Nanosheets: Photochemical Water Oxidation in the Quantum Confinement Regime. Chemistry of Materials, 2012, 24, 698-704.	6.7	158
32	Accelerated Synthesis and Discovery of Covalent Organic Framework Photocatalysts for Hydrogen Peroxide Production. Journal of the American Chemical Society, 2022, 144, 9902-9909.	13.7	154
33	Adsorption of a Catalytically Accessible Polyoxometalate in a Mesoporous Channel-type Metal–Organic Framework. Chemistry of Materials, 2017, 29, 5174-5181.	6.7	143
34	The potential for Bayesian compressive sensing to significantly reduce electron dose in high-resolution STEM images. Microscopy (Oxford, England), 2014, 63, 41-51.	1.5	140
35	Probing the Degradation Mechanisms in Electrolyte Solutions for Li-Ion Batteries by in Situ Transmission Electron Microscopy. Nano Letters, 2014, 14, 1293-1299.	9.1	137
36	Supported Molecular Iridium Catalysts: Resolving Effects of Metal Nuclearity and Supports as Ligands. Journal of the American Chemical Society, 2011, 133, 16186-16195.	13.7	132

#	Article	IF	CITATIONS
37	The Importance of Nanometric Passivating Films on Cathodes for Li–Air Batteries. ACS Nano, 2014, 8, 12483-12493.	14.6	131
38	Selective Methane Oxidation to Methanol on Cu-Oxo Dimers Stabilized by Zirconia Nodes of an NU-1000 Metal–Organic Framework. Journal of the American Chemical Society, 2019, 141, 9292-9304.	13.7	131
39	First demonstration of CdSe as a photocatalyst for hydrogen evolution from water under UV and visible light. Chemical Communications, 2008, , 2206.	4.1	127
40	Atomic-Scale Imaging and Spectroscopy for <i>In Situ</i> Liquid Scanning Transmission Electron Microscopy. Microscopy and Microanalysis, 2012, 18, 621-627.	0.4	125
41	Plasmonic Enhanced Emissions from Cubic NaYF ₄ :Yb:Er/Tm Nanophosphors. Chemistry of Materials, 2011, 23, 2987-2993.	6.7	124
42	Nanosecond time-resolved investigations using the in situ of dynamic transmission electron microscope (DTEM). Ultramicroscopy, 2008, 108, 1441-1449.	1.9	115
43	High-resolution low-dose scanning transmission electron microscopy. Journal of Electron Microscopy, 2010, 59, 103-112.	0.9	113
44	A site-isolated mononuclear iridium complex catalyst supported on MgO: Characterization by spectroscopy and aberration-corrected scanning transmission electron microscopy. Journal of Catalysis, 2010, 269, 318-328.	6.2	108
45	Selective Hydrodeoxygenation of Guaiacol Catalyzed by Platinum Supported on Magnesium Oxide. Catalysis Letters, 2012, 142, 1190-1196.	2.6	108
46	Diffusion mechanisms of native point defects in rutileTiO2:Ab initiototal-energy calculations. Physical Review B, 2007, 75, .	3.2	107
47	Practical considerations for high spatial and temporal resolution dynamic transmission electron microscopy. Ultramicroscopy, 2007, 107, 356-367.	1.9	99
48	K4Nb6O17-derived photocatalysts for hydrogen evolution from water: Nanoscrolls versus nanosheets. Journal of Solid State Chemistry, 2008, 181, 1678-1683.	2.9	98
49	A "Smart―Catalyst: Sinterâ€Resistant Supported Iridium Clusters Visualized with Electron Microscopy. Angewandte Chemie - International Edition, 2012, 51, 5929-5934.	13.8	97
50	Valence electron energy-loss spectroscopy in monochromated scanning transmission electron microscopy. Ultramicroscopy, 2005, 104, 176-192.	1.9	96
51	Dynamics of Soft Nanomaterials Captured by Transmission Electron Microscopy in Liquid Water. Journal of the American Chemical Society, 2014, 136, 1162-1165.	13.7	96
52	Direct <i>in Situ</i> Observation of Nanoparticle Synthesis in a Liquid Crystal Surfactant Template. ACS Nano, 2012, 6, 3589-3596.	14.6	93
53	Adsorption and diffusion of Pt and Au on the stoichiometric and reducedTiO2rutile (110) surfaces. Physical Review B, 2005, 72, .	3.2	92
54	Visualizing macromolecular complexes with in situ liquid scanning transmission electron microscopy. Micron, 2012, 43, 1085-1090.	2.2	89

4

#	Article	IF	CITATIONS
55	Femtosecond Ligand/Core Dynamics of Microwave-Assisted Synthesized Silicon Quantum Dots in Aqueous Solution. Journal of the American Chemical Society, 2011, 133, 20664-20667.	13.7	88
56	Photocatalytic Water Splitting with Suspended Calcium Niobium Oxides: Why Nanoscale is Better than Bulk – A Kinetic Analysis. Journal of Physical Chemistry C, 2012, 116, 3161-3170.	3.1	88
57	Interface Promoted Reversible Mg Insertion in Nanostructured Tin–Antimony Alloys. Advanced Materials, 2015, 27, 6598-6605.	21.0	88
58	Active and Stable Embedded Au@CeO ₂ Catalysts for Preferential Oxidation of CO. Chemistry of Materials, 2010, 22, 4335-4345.	6.7	87
59	Realizing the Full Potential of Insertion Anodes for Mg-Ion Batteries Through the Nanostructuring of Sn. Nano Letters, 2015, 15, 1177-1182.	9.1	87
60	Rational design of efficient electrode–electrolyte interfaces for solid-state energy storage using ion soft landing. Nature Communications, 2016, 7, 11399.	12.8	86
61	Towards an integrated materials characterization toolbox. Journal of Materials Research, 2011, 26, 1341-1383.	2.6	84
62	The impact of surface and retardation losses on valence electron energy-loss spectroscopy. Ultramicroscopy, 2008, 108, 84-99.	1.9	82
63	Towards full-structure determination of bimetallic nanoparticles with an aberration-corrected electron microscope. Nature Nanotechnology, 2010, 5, 843-847.	31.5	77
64	A Pyrene-4,5,9,10-Tetraone-Based Covalent Organic Framework Delivers High Specific Capacity as a Li-Ion Positive Electrode. Journal of the American Chemical Society, 2022, 144, 9434-9442.	13.7	77
65	Nanoclusters of Gold on a High-Area Support: Almost Uniform Nanoclusters Imaged by Scanning Transmission Electron Microscopy. ACS Nano, 2009, 3, 3691-3695.	14.6	75
66	Bridging Zirconia Nodes within a Metal–Organic Framework via Catalytic Ni-Hydroxo Clusters to Form Heterobimetallic Nanowires. Journal of the American Chemical Society, 2017, 139, 10410-10418.	13.7	74
67	Integrated Covalent Organic Framework/Carbon Nanotube Composite as Liâ€lon Positive Electrode with Ultraâ€High Rate Performance. Advanced Energy Materials, 2021, 11, 2101880.	19.5	73
68	An Astronomical 2175 A Feature in Interplanetary Dust Particles. Science, 2005, 307, 244-247.	12.6	70
69	A Bismuth Metal–Organic Framework as a Contrast Agent for X-ray Computed Tomography. ACS Applied Bio Materials, 2019, 2, 1197-1203.	4.6	68
70	Ferroelasticity in mixed conducting LaCoO3 based perovskites: a ferroelastic phase transition. Acta Materialia, 2003, 51, 5063-5071.	7.9	67
71	The Impact of Li Grain Size on Coulombic Efficiency in Li Batteries. Scientific Reports, 2016, 6, 34267.	3.3	67
72	Hydrogen Encapsulation in a Silicon Clathrate Type I Structure: Na _{5.5} (H ₂) _{2.15} Si ₄₆ :  Synthesis and Characterization. Journal of the American Chemical Society, 2007, 129, 13857-13862.	13.7	66

#	Article	IF	CITATIONS
73	Agglomerative Sintering of an Atomically Dispersed Ir ₁ /Zeolite Y Catalyst: Compelling Evidence Against Ostwald Ripening but for Bimolecular and Autocatalytic Agglomeration Catalyst Sintering Steps. ACS Catalysis, 2015, 5, 3514-3527.	11.2	66
74	Molecular Storage of Mg Ions with Vanadium Oxide Nanoclusters. Advanced Functional Materials, 2016, 26, 3446-3453.	14.9	65
75	Atomic Resolution Analysis of the Defect Chemistry and Microdomain Structure of Brownmilleriteâ€Type Strontium Cobaltite. Journal of the American Ceramic Society, 2002, 85, 969-976.	3.8	63
76	Minimum Cost Multi-Way Data Association for Optimizing Multitarget Tracking of Interacting Objects. IEEE Transactions on Pattern Analysis and Machine Intelligence, 2015, 37, 611-624.	13.9	60
77	Atomic and Electronic Structure of Mixed and Partial Dislocations in GaN. Physical Review Letters, 2005, 94, 025504.	7.8	59
78	Room temperature synthesis of surface-functionalised boron nanoparticles. Chemical Communications, 2007, , 580.	4.1	59
79	Atomicâ€Scale Determination of Active Facets on the MoVTeNb Oxide M1 Phase and Their Intrinsic Catalytic Activity for Ethane Oxidative Dehydrogenation. Angewandte Chemie - International Edition, 2016, 55, 8873-8877.	13.8	59
80	Design and synthesis of highly active MoVTeNb-oxides for ethane oxidative dehydrogenation. Nature Communications, 2019, 10, 4012.	12.8	59
81	Direct Evidence for Cation Nonâ€Stoichiometry and Cottrell Atmospheres Around Dislocation Cores in Functional Oxide Interfaces. Advanced Materials, 2010, 22, 2430-2434.	21.0	58
82	Co:CdS Diluted Magnetic Semiconductor Nanoparticles: Radiation Synthesis, Dopantâ^'Defect Complex Formation, and Unexpected Magnetism. Chemistry of Materials, 2008, 20, 440-446.	6.7	56
83	Quantification of the size-dependent energy gap of individual CdSe quantum dots by valence electron energy-loss spectroscopy. Ultramicroscopy, 2007, 107, 267-273.	1.9	55
84	Applying compressive sensing to TEM video: a substantial frame rate increase on any camera. Advanced Structural and Chemical Imaging, 2015, 1, .	4.0	55
85	Synthesis and characterization of Mg2Si/Si nanocomposites prepared from MgH2 and silicon, and their thermoelectric properties. Journal of Materials Chemistry, 2012, 22, 24805.	6.7	54
86	Hydrogen Activation and Metal Hydride Formation Trigger Cluster Formation from Supported Iridium Complexes. Journal of the American Chemical Society, 2012, 134, 5022-5025.	13.7	52
87	Understanding the Role of Solvation Forces on the Preferential Attachment of Nanoparticles in Liquid. ACS Nano, 2016, 10, 181-187.	14.6	51
88	Tracking Iridium Atoms with Electron Microscopy: First Steps of Metal Nanocluster Formation in One-Dimensional Zeolite Channels. Nano Letters, 2011, 11, 5537-5541.	9.1	49
89	Growth and structure of PbVO3 thin films. Applied Physics Letters, 2007, 90, 062903.	3.3	47
90	Mononuclear Zeolite-Supported Iridium: Kinetic, Spectroscopic, Electron Microscopic, and Size-Selective Poisoning Evidence for an Atomically Dispersed True Catalyst at 22 ŰC. ACS Catalysis, 2012, 2, 1947-1957.	11.2	47

#	Article	IF	CITATIONS
91	Gaining Control over Radiolytic Synthesis of Uniform Sub-3-nanometer Palladium Nanoparticles: Use of Aromatic Liquids in the Electron Microscope. Langmuir, 2016, 32, 1468-1477.	3.5	47
92	Low-dose aberration corrected cryo-electron microscopy of organic specimens. Ultramicroscopy, 2008, 108, 1636-1644.	1.9	46
93	<i>In-Situ</i> Electrochemical Transmission Electron Microscopy for Battery Research. Microscopy and Microanalysis, 2014, 20, 484-492.	0.4	45
94	Charge Separation in a Niobate Nanosheet Photocatalyst Studied with Photochemical Labeling. Langmuir, 2010, 26, 7254-7261.	3.5	44
95	Formation of Interfacial Layer and Long-Term Cyclability of Li–O ₂ Batteries. ACS Applied Materials & Interfaces, 2014, 6, 14141-14151.	8.0	44
96	Tracking Rh Atoms in Zeolite HY: First Steps of Metal Cluster Formation and Influence of Metal Nuclearity on Catalysis of Ethylene Hydrogenation and Ethylene Dimerization. Journal of Physical Chemistry Letters, 2016, 7, 2537-2543.	4.6	44
97	Improved Niobate Nanoscroll Photocatalysts for Partial Water Splitting. ChemSusChem, 2011, 4, 185-190.	6.8	43
98	Mesoscale Origin of the Enhanced Cycling-Stability of the Si-Conductive Polymer Anode for Li-ion Batteries. Scientific Reports, 2014, 4, 3684.	3.3	43
99	Oxide- and Zeolite-Supported Isostructural Ir(C ₂ H ₄) ₂ Complexes: Molecular-Level Observations of Electronic Effects of Supports as Ligands. Langmuir, 2012, 28, 12806-12815.	3.5	42
100	Formation of Oxygen Radical Sites on MoVNbTeOx by Cooperative Electron Redistribution. Journal of the American Chemical Society, 2017, 139, 12342-12345.	13.7	41
101	Site-isolated iridium complexes on MgO powder: individual Ir atoms imaged by scanning transmission electron microscopy. Chemical Communications, 2009, , 4657.	4.1	40
102	Photocatalytic Overall Water Splitting Under Visible Light Enabled by a Particulate Conjugated Polymer Loaded with Palladium and Iridium**. Angewandte Chemie - International Edition, 2022, 61, .	13.8	40
103	Anomalous Electrical Conductivity of Nanosheaves of CeO ₂ . Chemistry of Materials, 2009, 21, 1182-1186.	6.7	39
104	Decomposition Pathway of Ammonia Borane on the Surface of Nano-BN. Journal of Physical Chemistry C, 2010, 114, 13935-13941.	3.1	39
105	Chemical Stabilization and Electrochemical Destabilization of the Iron Keggin Ion in Water. Inorganic Chemistry, 2016, 55, 11078-11088.	4.0	39
106	Prospects for electron imaging with ultrafast time resolution. Applied Physics Letters, 2007, 90, 114101.	3.3	36
107	Structural variability of edge dislocations in a SrTiO ₃ low-angle [001] tilt grain boundary. Journal of Materials Research, 2009, 24, 2191-2199.	2.6	34
108	A (S)TEM Gas Cell Holder with Localized Laser Heating for <i>In Situ</i> Experiments. Microscopy and Microanalysis, 2013, 19, 470-478.	0.4	33

#	Article	IF	CITATIONS
109	Preferential growth of Pt on rutileTiO2. Physical Review B, 2006, 73, .	3.2	32
110	The origin of refractory minerals in comet 81P/Wild 2. Geochimica Et Cosmochimica Acta, 2009, 73, 7150-7161.	3.9	32
111	Using molecular dynamics to quantify the electrical double layer and examine the potential for its direct observation in the in-situ TEM. Advanced Structural and Chemical Imaging, 2015, 1, .	4.0	32
112	Minimising damage in high resolution scanning transmission electron microscope images of nanoscale structures and processes. Nanoscale, 2020, 12, 21248-21254.	5.6	32
113	Subsampled STEM-ptychography. Applied Physics Letters, 2018, 113, .	3.3	31
114	Ab initiostructural energetics of $\hat{l}^2 \hat{a}^3$ Si3N4surfaces. Physical Review B, 2005, 72, .	3.2	30
115	Chemical Inhomogeneity and Mixed-State Ferromagnetism in Diluted Magnetic Semiconductor Co:TiO2. Chemistry of Materials, 2008, 20, 1344-1352.	6.7	30
116	Atomic Resolution of the Structure of a Metal–Support Interface: Triosmium Clusters on MgO(110). Angewandte Chemie - International Edition, 2010, 49, 10089-10092.	13.8	30
117	Observing the colloidal stability of iron oxide nanoparticles <i>in situ</i> . Nanoscale, 2019, 11, 13098-13107.	5.6	30
118	Three-dimensionally intercrossing Mn3O4 nanowires. Acta Materialia, 2008, 56, 3516-3522.	7.9	29
119	Enabling direct nanoscale observations of biological reactions with dynamic TEM. Microscopy (Oxford, England), 2013, 62, 147-156.	1.5	29
120	Synthesis and Characterization of K _{8â~'<i>x</i>} (H ₂) _{<i>y</i>} Si ₄₆ . Inorganic Chemistry, 2010, 49, 815-822.	4.0	28
121	Intact and Fragmented Triosmium Clusters on MgO:  Characterization by X-ray Absorption Spectroscopy and High-Resolution Transmission Electron Microscopy. Journal of Physical Chemistry B, 2005, 109, 12738-12741.	2.6	27
122	lr ₆ Clusters Compartmentalized in the Supercages of Zeolite NaY: Direct Imaging of a Catalyst with Aberration-Corrected Scanning Transmission Electron Microscopy. ACS Catalysis, 2011, 1, 1613-1620.	11.2	27
123	Imaging Gold Atoms in Site-Isolated MgO-Supported Mononuclear Gold Complexes. Journal of Physical Chemistry C, 2009, 113, 16847-16849.	3.1	26
124	Quantifying transient states in materials with the dynamic transmission electron microscope. Journal of Electron Microscopy, 2010, 59, S67-S74.	0.9	26
125	Tip-Enhanced Raman Nanographs: Mapping Topography and Local Electric Fields. Nano Letters, 2015, 15, 2385-2390.	9.1	26
126	Prospects for analyzing the electronic properties in nanoscale systems by VEELS. Ultramicroscopy, 2008, 108, 270-276.	1.9	25

#	Article	IF	CITATIONS
127	Ultralow Contact Resistance at an Epitaxial Metal/Oxide Heterojunction Through Interstitial Site Doping. Advanced Materials, 2013, 25, 4001-4005.	21.0	24
128	Rhodium pair-sites on magnesium oxide: Synthesis, characterization, and catalysis of ethylene hydrogenation. Journal of Catalysis, 2016, 338, 12-20.	6.2	24
129	Probing 3â€D Structural Distortions and Coordination Changes at SrTiO ₃ Grain Boundaries Using Electron Energy Loss Spectroscopy. Journal of the American Ceramic Society, 1997, 80, 781-785.	3.8	23
130	Strongly driven crystallization processes in a metallic glass. Applied Physics Letters, 2009, 94, .	3.3	23
131	Automatic recovery of missing amplitudes and phases in tilt-limited electron crystallography of two-dimensional crystals. Physical Review E, 2011, 84, 011916.	2.1	23
132	Liquid Cell Transmission Electron Microscopy Sheds Light on The Mechanism of Palladium Electrodeposition. Langmuir, 2019, 35, 862-869.	3.5	23
133	Measuring the hole-state anisotropy inMgB2by electron energy-loss spectroscopy. Physical Review B, 2003, 67, .	3.2	22
134	Pyromorphite Growth on Lead-Sulfide Surfaces. Environmental Science & Technology, 2004, 38, 5529-5534.	10.0	22
135	DC Photoelectron Gun Parameters for Ultrafast Electron Microscopy. Microscopy and Microanalysis, 2009, 15, 298-313.	0.4	22
136	Sinter-Resistant Catalysts: Supported Iridium Nanoclusters with Intrinsically Limited Sizes. Catalysis Letters, 2012, 142, 1445-1451.	2.6	22
137	Examining Elemental Surface Enrichment in Ultrafine Aerosol Particles Using Analytical Scanning Transmission Electron Microscopy. Aerosol Science and Technology, 2004, 38, 365-381.	3.1	21
138	Determination of Nanocluster Sizes from Dark-Field Scanning Transmission Electron Microscopy Images. Journal of Physical Chemistry C, 2008, 112, 1759-1763.	3.1	21
139	Laserâ€based in situ techniques: Novel methods for generating extreme conditions in TEM samples. Microscopy Research and Technique, 2009, 72, 122-130.	2.2	21
140	Atomically Resolved Site-Isolated Catalyst on MgO: Mononuclear Osmium Dicarbonyls formed from Os ₃ (CO) ₁₂ . Journal of Physical Chemistry Letters, 2012, 3, 1865-1871.	4.6	21
141	Site-Isolated Molecular Iridium Complex Catalyst Supported in the 1-Dimensional Channels of Zeolite HSSZ-53: Characterization by Spectroscopy and Aberration-Corrected Scanning Transmission Electron Microscopy. ACS Catalysis, 2012, 2, 1002-1012.	11.2	21
142	Direct atomic scale analysis of the distribution of Cu valence states in Cu/γ-Al2O3 catalysts. Applied Catalysis B: Environmental, 2002, 38, 271-281.	20.2	20
143	Investigation of the effect of varying growth pauses on the structural and optical properties of InAs/GaAs quantum dot heterostructures. Superlattices and Microstructures, 2009, 46, 611-617.	3.1	20
144	Simulating realistic imaging conditions for in situ liquid microscopy. Ultramicroscopy, 2013, 135, 36-42.	1.9	20

#	Article	IF	CITATIONS
145	Electric field enhancement in a self-assembled 2D array of silver nanospheres. Journal of Chemical Physics, 2014, 141, 214308.	3.0	20
146	Microstructure investigations of Yb- and Bi-doped Mg2Si prepared from metal hydrides for thermoelectric applications. Journal of Solid State Chemistry, 2017, 245, 152-159.	2.9	20
147	Catalytic Consequences of Particle Size and Chloride Promotion in the Ring-Opening of Cyclopentane on Pt/Al ₂ O ₃ . ACS Catalysis, 2013, 3, 328-338.	11.2	19
148	Tuning interfacial exchange interactions via electronic reconstruction in transition-metal oxide heterostructures. Applied Physics Letters, 2016, 109, .	3.3	19
149	<i>In situ</i> electrochemical scanning/transmission electron microscopy of electrode–electrolyte interfaces. MRS Bulletin, 2020, 45, 738-745.	3.5	19
150	Direct Formation of Mesoporous Coesite Single Crystals from Periodic Mesoporous Silica at Extreme Pressure. Angewandte Chemie - International Edition, 2010, 49, 4301-4305.	13.8	18
151	Direct Visualization of Aggregate Morphology and Dynamics in a Model Soil Organic–Mineral System. Environmental Science and Technology Letters, 2017, 4, 186-191.	8.7	18
152	Single‣ite Osmium Catalysts on MgO: Reactivity and Catalysis of CO Oxidation. Chemistry - A European Journal, 2017, 23, 2532-2536.	3.3	18
153	Nanoparticle Immobilization for Controllable Experiments in Liquid-Cell Transmission Electron Microscopy. ACS Applied Materials & Interfaces, 2018, 10, 22801-22808.	8.0	18
154	Analysis of extraterrestrial particles using monochromated electron energy-loss spectroscopy. Micron, 2005, 36, 369-379.	2.2	17
155	Application of two-dimensional crystallography and image processing to atomic resolution Z-contrast images. Journal of Electron Microscopy, 2009, 58, 223-244.	0.9	17
156	Gold Cluster Diffusion Kinetics on Stoichiometric and Reduced Surfaces of Rutile TiO ₂ (110). Journal of Physical Chemistry C, 2011, 115, 11611-11617.	3.1	17
157	Threeâ€Dimensional Structural Analysis of MgOâ€Supported Osmium Clusters by Electron Microscopy with Singleâ€Atom Sensitivity. Angewandte Chemie - International Edition, 2013, 52, 5262-5265.	13.8	17
158	Distribution of Metal Cations in Niâ€Moâ€W Sulfide Catalysts. ChemCatChem, 2015, 7, 3692-3704.	3.7	17
159	Electron Microscopy Investigations of Nanostructured Ce/Mn Oxides for Catalytic Wet Oxidation. Journal of Physical Chemistry C, 2010, 114, 8981-8991.	3.1	16
160	Segregation of Mn2+Dopants as Interstitials in SrTiO3Grain Boundaries. Materials Research Letters, 2014, 2, 16-22.	8.7	16
161	Enhanced Interface-Driven Perpendicular Magnetic Anisotropy by Symmetry Control in Oxide Superlattices. Physical Review Applied, 2021, 15, .	3.8	16
162	Characterization of oxygen ordering in (La, Sr)FeO3 – Î'by atomic resolution Zâ€contrast imaging and electron energyâ€loss spectroscopy. Journal of Electron Microscopy, 2002, 51, S59-S66.	0.9	16

#	Article	IF	CITATIONS
163	In Situ Laser Synthesis of Si Nanowires in the Dynamic TEM. Small, 2008, 4, 2187-2190.	10.0	15
164	Atomic and electronic structures of the SrVO3-LaAlO3 interface. Journal of Applied Physics, 2011, 110, 046104.	2.5	15
165	Tuning magnetic and transport properties through strain engineering in La0.7Sr0.3MnO3/La0.5Sr0.5TiO3 superlattices. Journal of Applied Physics, 2012, 111, 084906.	2.5	15
166	Advantages of MgAlO _{<i>x</i>} over γ-Al ₂ O ₃ as a Support Material for Potassium-Based High-Temperature Lean NO _{<i>x</i>} Traps. ACS Catalysis, 2015, 5, 4680-4689.	11.2	15
167	Controlling radiolysis chemistry on the nanoscale in liquid cell scanning transmission electron microscopy. Physical Chemistry Chemical Physics, 2021, 23, 17766-17773.	2.8	15
168	Sub-Sampled Imaging for STEM: Maximising Image Speed, Resolution and Precision Through Reconstruction Parameter Refinement. Ultramicroscopy, 2022, 233, 113451.	1.9	15
169	Point defect characterization in HAADF-STEM images using multivariate statistical analysis. Ultramicroscopy, 2011, 111, 251-257.	1.9	14
170	Quantitative <i>Z</i> â€Contrast Imaging of Supported Metal Complexes and Clusters—A Gateway to Understanding Catalysis on the Atomic Scale. ChemCatChem, 2013, 5, 2673-2683.	3.7	14
171	In Situ Observation of Directed Nanoparticle Aggregation During the Synthesis of Ordered Nanoporous Metal in Soft Templates. Chemistry of Materials, 2014, 26, 1426-1433.	6.7	14
172	Fabrication of electrocatalytic Ta nanoparticles by reactive sputtering and ion soft landing. Journal of Chemical Physics, 2016, 145, 174701.	3.0	14
173	Synthesis and spectroscopic characterization of P-doped Na4Si4. Journal of Solid State Chemistry, 2010, 183, 2522-2527.	2.9	13
174	Quantifying the low-energy limit and spectral resolution in valence electron energy loss spectroscopy. Ultramicroscopy, 2013, 124, 130-138.	1.9	13
175	DRILL Interface Makes Ion Soft Landing Broadly Accessible for Energy Science and Applications. Batteries and Supercaps, 2018, 1, 97-101.	4.7	13
176	Iridium Complexes and Clusters in Dealuminated Zeolite HY: Distribution between Crystalline and Impurity Amorphous Regions. ACS Catalysis, 2014, 4, 2662-2666.	11.2	12
177	Migration of Single Iridium Atoms and Tri-iridium Clusters on MgO Surfaces: Aberration-Corrected STEM Imaging and Ab Initio Calculations. Journal of Physical Chemistry Letters, 2015, 6, 4675-4679.	4.6	12
178	Triosmium Clusters on a Support: Determination of Structure by Xâ€ r ay Absorption Spectroscopy and Highâ€Resolution Microscopy. Chemistry - A European Journal, 2011, 17, 1000-1008.	3.3	11
179	Zeolite-supported bimetallic catalyst: controlling selectivity of rhodium complexes by nearby iridium complexes. Catalysis Science and Technology, 2013, 3, 2199.	4.1	11
180	Synthesis and characterization of P-doped amorphous and nanocrystalline Si. Polyhedron, 2013, 58, 156-161.	2.2	11

#	Article	IF	CITATIONS
181	Magnetism and transport in transparent high-mobility <mml:math xmlns:mml="http://www.w3.org/1998/Math/MathML"> <mml:msub> <mml:mi>BaSnO </mml:mi> <mml:mn>3 films doped with La, Pr, Nd, and Gd. Physical Review Materials, 2019, 3, .</mml:mn></mml:msub></mml:math 	ml2man> </td <td>mmlımsub></td>	mml ı msub>
182	Electron Microscopy and Spectroscopy on the Ultrafast Timescale. ChemPhysChem, 2010, 11, 781-782.	2.1	10
183	General schema for [001] tilt grain boundaries in dense packing cubic crystals. Acta Materialia, 2013, 61, 3392-3398.	7.9	10
184	Energetics of CdSxSe1â^'x quantum dots in borosilicate glasses. Journal of Non-Crystalline Solids, 2007, 353, 2785-2795.	3.1	9
185	Symposium on Ultrafast Electron Microscopy and Ultrafast Science. Microscopy and Microanalysis, 2009, 15, 271-271.	0.4	9
186	Quality of Graphite Target for Biological/Biomedical/Environmental Applications of ¹⁴ C-Accelerator Mass Spectrometry. Analytical Chemistry, 2010, 82, 2243-2252.	6.5	9
187	Structural variability in La0.5Sr0.5TiO3 $\hat{A}\pm\hat{I}$ thin films. Applied Physics Letters, 2011, 99, 261907.	3.3	9
188	Imaging individual lanthanum atoms in zeolite Y by scanning transmission electron microscopy: Evidence of lanthanum pair sites. Microporous and Mesoporous Materials, 2015, 213, 95-99.	4.4	9
189	Practical Implementation of Compressive Sensing for High Resolution STEM. Microscopy and Microanalysis, 2016, 22, 558-559.	0.4	9
190	The Role of Gas in Determining Image Quality and Resolution During Inâ€Situ Scanning Transmission Electron Microscopy Experiments. ChemCatChem, 2017, 9, 3478-3485.	3.7	9
191	Structural Transformations in self-assembled Semiconductor Quantum Dots as inferred by Transmission Electron Microscopy. , 2002, 4807, 71.		8
192	Investigating the Structureâ€Property Relationships at Grain Boundaries in MgO Using Bondâ€Valence Pair Potentials and Multiple Scattering Analysis. Journal of the American Ceramic Society, 1999, 82, 366-372.	3.8	8
193	A comprehensive study of the effect of in situ annealing at high growth temperature on the morphological and optical properties of self-assembled InAs/GaAs QDs. Applied Physics A: Materials Science and Processing, 2009, 95, 713-720.	2.3	8
194	Nearly Uniform Decaosmium Clusters Supported on MgO: Characterization by X-ray Absorption Spectroscopy and Scanning Transmission Electron Microscopy. Journal of Physical Chemistry C, 2009, 113, 13377-13385.	3.1	8
195	Timeâ€Resolved Annular Dark Field Imaging of Catalyst Nanoparticles. ChemPhysChem, 2010, 11, 2088-2090.	2.1	8
196	Compressive STEM-EELS. Microscopy and Microanalysis, 2016, 22, 560-561.	0.4	8
197	High temporal-resolution scanning transmission electron microscopy using sparse-serpentine scan pathways. Scientific Reports, 2021, 11, 22722.	3.3	8
198	Chemistry of Tantalum Clusters in Solution and on SiO ₂ Supports:  Analogies and Contrasts. Langmuir, 2007, 23, 8845-8854.	3.5	7

#	Article	IF	CITATIONS
199	Investigation on Thickness Effect of Ultrathin Vinylidene Fluoride/Trifluoroethylene Copolymer Films. Japanese Journal of Applied Physics, 2011, 50, 09NA05.	1.5	7
200	The Complex Role of Aluminium Contamination in Nickelâ€Rich Layered Oxide Cathodes for Lithiumâ€Ion Batteries. Batteries and Supercaps, 2021, 4, 1813-1820.	4.7	7
201	Photocatalytic Overall Water Splitting Under Visible Light Enabled by a Particulate Conjugated Polymer Loaded with Palladium and Iridium**. Angewandte Chemie, 2022, 134, .	2.0	7
202	Atomic Scale Characterization of Vacancy Ordering in Oxygen Conducting Membranes. Microscopy and Microanalysis, 2002, 8, 475-486.	0.4	6
203	Electronic and superconducting properties of oxygen-orderedMgB2compounds of the formMg2B3Ox. Physical Review B, 2004, 70, .	3.2	6
204	Recognition of melting of nanoparticle catalysts with cubically shaped Co3O4 nanoparticles. Journal of Colloid and Interface Science, 2008, 321, 251-255.	9.4	6
205	Tantalum Clusters Supported on Silicaâ^Alumina: Influence of Support Composition and Chemistry on Cluster Structure. Langmuir, 2009, 25, 10754-10763.	3.5	6
206	Strain relaxation defects in perovskite oxide superlattices. Journal of Materials Research, 2012, 27, 1436-1444.	2.6	6
207	Phase transition singled out. Nature Chemistry, 2013, 5, 363-364.	13.6	6
208	Antisite defects in La0.7Sr0.3MnO3 and La0.7Sr0.3FeO3. Applied Physics Letters, 2013, 102, 151911.	3.3	6
209	Microdomain Formation, Oxidation, and Cation Ordering in LaCa 2 Fe 3 O 8+ y. Journal of the American Ceramic Society, 2015, 98, 2248-2254.	3.8	6
210	Si 0.85 Ge 0.15 oxynitridation in nitric oxide/nitrous oxide ambient. Journal of Applied Physics, 2003, 94, 716-719.	2.5	5
211	Experimental and theoretical improvements on understanding of the O K-edge of TeO2. Ultramicroscopy, 2006, 106, 123-129.	1.9	5
212	Yttria-stabilized zirconia crystallization in Al ₂ O ₃ /YSZ multilayers. Journal of Materials Research, 2012, 27, 939-943.	2.6	5
213	Cation uniformity and magnetic properties of La0.7Sr0.3Mn0.5Fe0.5O3 thin films. Journal of Magnetism and Magnetic Materials, 2013, 325, 69-74.	2.3	5
214	Symmetries of migrationâ€related segments of all [001] coincidence site lattice tilt boundaries in (001) projection for all holohedral cubic materials. Crystal Research and Technology, 2014, 49, 708-720.	1.3	5
215	Structure of catalyst particles from in-situ electron microscopy: a web themed issue. Chemical Communications, 2014, 50, 12417-12419.	4.1	5
216	Understanding the Effect of Additives in Li-ion and Li-Sulfur Batteries by Operando ec- (S)TEM. Microscopy and Microanalysis, 2016, 22, 22-23.	0.4	5

#	Article	IF	CITATIONS
217	Directional Statistics of Preferential Orientations of Two Shapes in Their Aggregate and Its Application to Nanoparticle Aggregation. Technometrics, 2018, 60, 332-344.	1.9	5
218	Microstructural evolution of protective La–Cr–O films studied by transmission electron microscopy. Journal of Solid State Electrochemistry, 2006, 10, 659-662.	2.5	4
219	Effect of InAlGaAs and GaAs Combination Barrier Thickness on the Duration of Dot Formation in Different Layers of Stacked InAs/GaAs Quantum Dot Heterostructure Grown by MBE. Journal of Nanoscience and Nanotechnology, 2010, 10, 5202-5206.	0.9	4
220	TEM Video Compressive Sensing. Microscopy and Microanalysis, 2015, 21, 1583-1584.	0.4	4
221	Atomic Ordering in Self-assembled Epitaxial II-VI and IV-VI Compound Semiconductor Quantum Dot Systems. Materials Research Society Symposia Proceedings, 2002, 749, 1.	0.1	3
222	Compressive Sensing in Microscopy: a Tutorial. Microscopy and Microanalysis, 2016, 22, 2084-2085.	0.4	3
223	Enhanced Longâ€Term Cathode Stability by Tuning Interfacial Nanocomposite for Intermediate Temperature Solid Oxide Fuel Cells. Advanced Materials Interfaces, 2022, 9, .	3.7	3
224	Atomic scale defect analysis in the scanning transmission electron microscope. Microscopy Research and Technique, 2006, 69, 330-342.	2.2	2
225	The Hydrogen Evolution Reaction: Water Reduction Photocatalysis—Improved Niobate Nanoscroll Photocatalysts for Partial Water Splitting. Springer Theses, 2014, , 9-25.	0.1	2
226	In-Situ Liquid Transmission Electron Microscopy (TEM) for the analysis of Metal Organic Frameworks (MOFs). Microscopy and Microanalysis, 2014, 20, 1614-1615.	0.4	2
227	Implementing Sub-sampling Methods for Low-Dose (Scanning) Transmission Electron Microscopy (S/TEM). Microscopy and Microanalysis, 2017, 23, 82-83.	0.4	2
228	Acquisition of STEM Images by Adaptive Compressive Sensing. Microscopy and Microanalysis, 2017, 23, 96-97.	0.4	2
229	The Effect of Gas on Image Quality and Resolution in In situ Scanning Transmission Electron Microscopy. Microscopy and Microanalysis, 2017, 23, 916-917.	0.4	2
230	Implementing Sparse Sub-Sampling Methods for Low-Dose/High Speed STEM. Microscopy and Microanalysis, 2018, 24, 1952-1953.	0.4	2
231	The Merits of In situ Environmental STEM for the Study of Complex Oxide Catalysts at Work. Microscopy and Microanalysis, 2018, 24, 238-239.	0.4	2
232	Event detection for undersampled electron microscopy experiments: A control chart case study. Quality Engineering, 2020, 32, 244-254.	1.1	2
233	The Potential Benefits of Compressed Sensing and Machine Learning for Advanced Imaging and Spectroscopy in the Electron Microscope. Microscopy and Microanalysis, 2020, 26, 2458-2460.	0.4	2
234	Quantifying the Effects of Beam Overlap on Radiation Damage via Radiolysis Products in the <i>In-situ</i> Liquid (S)TEM Cell. Microscopy and Microanalysis, 2020, 26, 2572-2574.	0.4	2

1

239 Z-Contrast STEM Imaging and Ab-Initio Calculations of Grain Boundaries in SrTiO3. Materials Research 0.1 1 236 Atomic Self-ordering in Hetersenthicially Grave Semiconductor Quantum Dots due to Relaxation of External Lattice Mismatch Strains. Materials Research Society Symposia Proceedings, 2001, 696, 1. 0.1 1 237 Atomic Self-ordering in Hetersenthicially Grave Semiconductor Quantum Dots Due to Relaxation of Electron Materials Research Society Symposia Proceedings, 2001, 707, 881. 0.1 1 238 Nominal POSe nano-tslands on PDTe: grown by MBE, analyzed by AFM and TEM. Materials Research 0.1 1 239 Detringuishing Intra-band and Inter-band Transitions in Mg8 esub 24/stub Using Monochromated FELS. 0.4 1 240 Supported Metal Catalyst Interfaces and Stability in TEM Imaging. Microscopy and Microanalysis, 2004, 0.4 1 241 Identifying unknown nanocrystals by three Ingravititing in two dimensions and free access 1 242 Above Room-Temperature Ferromagnetism in CsN Powders by Calcinations with CuO. Materials 0.1 1 243 Install State Physics, 2010, 7, 9, 12. 0.8 1 244 Photocatalytic water splitting with nano K 4 Nb 6 O 17. Proceedings of SPIE, 2010, 0.8 1 245 Insold State Physics, 2010, 7, 9, 12. 0.4 1 <th>#</th> <th>Article</th> <th>IF</th> <th>CITATIONS</th>	#	Article	IF	CITATIONS
246 External Lattice Mismatch Strains. Materials Research Society Symposia Proceedings, 2001, 696, 1. 0.1 1 247 Atomic Self-Ordering in Heteroepitaxially Grown Semiconductor Quantum Dots Due to Relaxation of External Lattice Mannatch Strains. Materials Research Society Symposia Proceedings, 2001, 707, 881. 0.1 1 248 Nominal PbSe nano-Islands on PbTe: grown by MBE, analyzed by AFM and TEM. Materials Research 0.1 1 249 Distinguishing Initia-band and Inter-band Transitions in MgB stabs 22/stabs Using Monochromated EELS. 0.4 1 240 Supported Metal Catalyst Interfaces and Stability in TEM Imaging. Microscopy and Microanalysis, 2004, 0.4 1 241 Identifying unknown nanocrystals by fringe fingerprinting in two dimensions and free-access 1 1 242 Above Room-Temperature Forromagnetism in CaN Powders by Calcinations with CuO. Materials 0.1 1 243 Initial oxidation of InN quantum dots the role of cubic InN. Physica Status Solid C: Current Topics 0.6 1 244 Photocatalytic water splitting with Multi-Component Catalystis: Proposed Mechanism of Charge Transport 0.1 1 243 In Situ Observation of Directed Nanoparticle Aggregation During the Synthesis of Ordered 0.4 1 244 Photocatalytic water splitting with Multi-Co	235		0.1	1
237 External Lattice Mismatch Strains. Materials Research Society Symposia Proceedings, 2001, 707, 881. 0.1 1 238 Nominal PbSe nano-islands on PbTe; grown by MBE, analyzed by AFM and TEM. Materials Research Society Symposia Proceedings, 2004, 829, 467. 0.1 1 239 Distinguishing Intra-band and Interchand Transitions in Mg8 (subs 2.4 subs Using Monochromated EELS. 0.4 1 240 Supported Metal Catalyst Interfaces and Stability in TEM Imaging. Microscopy and Microanalysis, 2004, 0.4 1 241 Identifying unknown nanocrystals by fringe fingerprinting in two dimensions and free-access 1 242 Above Room-Temperature Ferromagnetism in GaN Powders by Calcinations with CuO. Materials 0.1 1 243 Natural oxidation of InN quantum dots: the role of cubic InN. Physica Status Solidi C: Current Topics 0.8 1 244 Photocatalytic water splitting with nano-K 4 Nb 6 O 17. Proceedings of SPIE, 2010, 0.8 1 245 Complete Water Splitting with Nulti-Component Catalysts Proposed Mechanism of Charge Transport 0.1 1 246 In Situ Observation of Directed Nanoparticle Aggregation During the Synthesis of Ordered 0.4 1 247 In Situ Observation of Directed Nanoparticle Aggregation During the Synthesis of Ordered 0.4 1	236	Atomic Self-ordering in Heteroepitaxially Grown Semiconductor Quantum Dots due to Relaxation of External Lattice Mismatch Strains. Materials Research Society Symposia Proceedings, 2001, 696, 1.	0.1	1
238 Society Symposia Proceedings, 2004, 829, 467. 0.1 1 239 Distinguishing Intra-band and Inter-band Transitions in Mg8/sub>2x/sub>2x/sub> Using Monochromated EELS. 0.4 1 240 Supported Metal Catalyst Interfaces and Stability in TEM Imaging. Microscopy and Microanalysis, 2004, 0.4 1 241 Identifying unknown nanocrystals by fringe friggerprinting in two dimensions and free-access 1 242 Above Room-Temperature Ferromagnetism in CaN Powders by Calcinations with CuO. Materials 0.1 1 242 Above Room-Temperature Ferromagnetism in CaN Powders by Calcinations with CuO. Materials 0.1 1 243 Natural oxidation of InN quantum dots: the role of cubic InN. Physica Status Solidi C: Current Topics 0.8 1 244 Photocatalytic water splitting with nano-K 4 Nb 6 0 17. Proceedings of SPIE, 2010, 0.8 1 245 Complete Water Splitting with Multi-Component Catalyste: Proposed Machanism of Charge Transport 0.1 1 246 In Situ Observation of Directed Nanoparticle Aggregation During the Synthesis of Ordered 0.4 1 247 Implementing in situ Experiments in Liquids in the (Scanning) Transmission Electron Microscopy and Microanalysis, 2014, 20, 1648-1649. 0.4 1 246 In Situ Observation	237		0.1	1
259 Microscopy and Microanalysis, 2004, 10, 840-841. 0.4 1 240 Supported Metal Catalyst Interfaces and Stability in TEM Imaging. Microscopy and Microanalysis, 2004, 0,4 1 241 Identifying unknown nanocrystals by fringe fringerprinting in two dimensions and free-access crystallographic databases, 2005, 6000, 206. 1 242 Above Room-Temperature Ferromagnetism in GaN Powders by Calcinations with CuO. Materials 0.1 1 243 Research Society Symposia Proceedings, 2006, 941, 1. 0.1 1 244 Natural oxidation of InN quantum dots: the role of cubic InN. Physica Status Solidi C: Current Topics 0.8 1 244 Photocatalytic water splitting with nano-K 4 Nb 6 O 17. Proceedings of SPIE, 2010, , . 0.8 1 245 Complete Water Splitting with Multi-Component Catalysts: Proposed Mechanism of Charge Transport in NCX Loaded SrTiO3 Photocatalyst for Complete Water Splitting. Springer Theses, 2014, 53-66. 0.1 1 246 In Silu Observation of Directed Nanoparticle Aggregation During the Synthesis of Ordered Nanopartice Materian Complexes With Single-Atom Sensitivity. Microscopy and Microanalysis, 2014, 20, 1600-1601. 0.4 1 247 Implementing in situ Experiments in Liquids in the (Scanning) Transmission Electron Microscope (STEM) and Pyramic TEM (DIEM). Microscopy and Microanalysis, 2014, 20, 1648-1649. 0.4 1	238		0.1	1
240 10, 448.449. 0.4 1 241 Identifying unknown nanocrystals by fringe fingerprinting in two dimensions and free-access 1 241 Identifying unknown nanocrystals by fringe fingerprinting in two dimensions and free-access 1 242 Above Room-Temperature Ferromagnetism in GaN Powders by Calcinations with CuO. Materials 0.1 1 242 Above Room-Temperature Ferromagnetism in GaN Powders by Calcinations with CuO. Materials 0.1 1 243 Natural oxidation of InN quantum dots: the role of cubic InN. Physica Status Solidi C: Current Topics 0.8 1 244 Photocatalytic water splitting with nano-K 4 Nb 6 O 17. Proceedings of SPIE, 2010, 0.8 1 245 Complete Water Splitting with Multi-Component Catalysts: Proposed Mechanism of Charge Transport in Nick Loaded SrTiO3 Photocatalyst for Complete Water Splitting. Springer Theses, 2014, 53-66. 0.1 1 246 In Situ Observation of Directed Nanoparticle Aggregation During the Synthesis of Ordered Nanoporous Metal in Soft Templates. Microscopy and Microanalysis, 2014, 20, 1600-1601. 0.4 1 247 (Inplementing in stu Experiments in Liquids in the (Scanning) Transmission Electron Microscope (ISTEM) and Dynamic TEM (OTEM). Microscopy and Microanalysis, 2014, 20, 1648-1649. 0.4 1 248 Metal Clusters and Single-metal at	239		0.4	1
241 crystallographic databases. , 2005, 6000, 206. 1 242 Above Room-Temperature Ferromagnetism in GaN Powders by Calcinations with CuO. Materials 0.1 1 242 Above Room-Temperature Ferromagnetism in GaN Powders by Calcinations with CuO. Materials 0.1 1 243 Natural oxidation of InN quantum dots: the role of cubic InN. Physica Status Solidi C: Current Topics 0.8 1 244 Photocatalytic water splitting with nano-K 4 Nb 6 O 17. Proceedings of SPIE, 2010, , . 0.8 1 245 Complete Water Splitting with Multi-Component Catalysts: Proposed Mechanism of Charge Transport in NIOX Loaded SrTIO3 Photocatalyst for Complete Water Splitting. Springer Theses, 2014, , 53-66. 0.1 1 246 In Situ Observation of Directed Nanoparticle Aggregation During the Synthesis of Ordered Nanoporous Metal in Soft Templates. Microscopy and Microanalysis, 2014, 20, 1600-1601. 0.4 1 247 Implementing in situ Experiments in Liquids in the (Scanning) Transmission Electron Microscope ((S)TEM) and Dynamic TEM (DTEM). Microscopy and Microanalysis, 2014, 20, 1648-1649. 0.4 1 248 Quantitative Z-contrast Imaging in Scanning Transmission Electron Microscopy of Zeolite-supported Metal Clusters and Single-metal-atom Complexes With Single-Atom Sensitivity. Microscopy and Microanalysis, 2014, 20, 148-149. 0.4 1 249 Ex Situ and In Situ (S)TEM	240	Supported Metal Catalyst Interfaces and Stability in TEM Imaging. Microscopy and Microanalysis, 2004, 10, 448-449.	0.4	1
242 Research Society Symposia Proceedings, 2006, 941, 1. 0.1 1 243 Natural oxidation of InN quantum dots: the role of cubic InN. Physica Status Solidi C: Current Topics 0.8 1 244 Photocatalytic water splitting with nano-K 4 Nb 6 O 17. Proceedings of SPIE, 2010, , . 0.8 1 245 Complete Water Splitting with Multi-Component Catalysts: Proposed Mechanism of Charge Transport in NIOx Loaded STIO3 Photocatalyst for Complete Water Splitting, Springer Theses, 2014, , 53-66. 0.1 1 246 In Situ Observation of Directed Nanoparticle Aggregation During the Synthesis of Ordered Nanoporous Metal in Soft Templates. Microscopy and Microanalysis, 2014, 20, 1600-1601. 0.4 1 247 Implementing in situ Experiments in Liquids in the (Scanning) Transmission Electron Microscope ((S)TEM) and Dynamic TEM (DTEM). Microscopy and Microanalysis, 2014, 20, 1648-1649. 0.4 1 248 Metal Clusters and Single-metal-atom Complexes With Single-Atom Sensitivity. Microscopy and Microanalysis, 2014, 20, 148-1649. 0.4 1 249 Ex Situ and In Situ (S)TEM of Iron Oxide Nanoparticles Synthesized by Decomposition of an Organometallic Precursor. Microscopy and Microanalysis, 2015, 21, 965-966. 0.4 1 250 Revealing the Working Active Sites of M1 phase for Ethane Oxidation. Microscopy and Microanalysis, 2016, 22, 790-791. 0.4 1 251	241			1
243 in Solid State Physics, 2010, 7, 9-12. 0.8 1 244 Photocatalytic water splitting with nano-K 4 Nb 6 O 17. Proceedings of SPIE, 2010, , . 0.8 1 244 Photocatalytic water splitting with Multi-Component Catalysts: Proposed Mechanism of Charge Transport in NiOx Loaded StTiO3 Photocatalyst for Complete Water Splitting, Springer Theses, 2014, , 53-66. 0.1 1 246 In Situ Observation of Directed Nanoparticle Aggregation During the Synthesis of Ordered Nanoporous Metal in Soft Templates. Microscopy and Microanalysis, 2014, 20, 1600-1601. 0.4 1 247 Implementing in situ Experiments in Liquids in the (Scanning) Transmission Electron Microscope ((S)TEM) and Dynamic TEM (DTEM). Microscopy and Microanalysis, 2014, 20, 1648-1649. 0.4 1 248 Quantitative Z-contrast Imaging in Scanning Transmission Electron Microscopy of Zeolite-supported Metal Clusters and Single-metal-atom Complexes With Single-Atom Sensitivity. Microscopy and Microanalysis, 2014, 20, 148-149. 0.4 1 249 Ex Situ and In Situ (S)TEM of Iron Oxide Nanoparticles Synthesized by Decomposition of an Organometallic Precursor. Microscopy and Microanalysis, 2015, 21, 965-966. 0.4 1 250 Revealing the Working Active Sites of M1 phase for Ethane Oxidation. Microscopy and Microanalysis, 2016, 22, 790-791. 0.4 1 251 The Mechanisms for Preferential Attachment of Nanoparticles in Liquid Determined Using Liquid Ce	242		0.1	1
245Complete Water Splitting with Multi-Component Catalysts: Proposed Mechanism of Charge Transport in NiOx Loaded SrTiO3 Photocatalyst for Complete Water Splitting. Springer Theses, 2014, 53-66.0.11246In Situ Observation of Directed Nanoparticle Aggregation During the Synthesis of Ordered Nanoporous Metal in Soft Templates. Microscopy and Microanalysis, 2014, 20, 1600-1601.0.41247Implementing in situ Experiments in Liquids in the (Scanning) Transmission Electron Microscope (IS)TEM) and Dynamic TEM (DTEM). Microscopy and Microanalysis, 2014, 20, 1648-1649.0.41248Quantitative Z-contrast Imaging in Scanning Transmission Electron Microscopy of Zeolite-supported Metal Clusters and Single-metal-atom Complexes With Single-Atom Sensitivity. Microscopy and Microanalysis, 2014, 20, 148-149.0.41249Ex Situ and In Situ (S)TEM of Iron Oxide Nanoparticles Synthesized by Decomposition of an Organometallic Precursor. Microscopy and Microanalysis, 2015, 21, 965-966.0.41250Revealing the Working Active Sites of M1 phase for Ethane Oxidation. Microscopy and Microanalysis, 2016, 22, 790-791.0.41	243	Natural oxidation of InN quantum dots: the role of cubic InN. Physica Status Solidi C: Current Topics in Solid State Physics, 2010, 7, 9-12.	0.8	1
243in NiOx Loaded SrTiO3 Photocatalyst for Complete Water Splitting. Springer Theses, 2014, 53-66.0.11246In Situ Observation of Directed Nanoparticle Aggregation During the Synthesis of Ordered Nanoporous Metal in Soft Templates. Microscopy and Microanalysis, 2014, 20, 1600-1601.0.41247Implementing in situ Experiments in Liquids in the (Scanning) Transmission Electron Microscope ((S)TEM) and Dynamic TEM (DTEM). Microscopy and Microanalysis, 2014, 20, 1648-1649.0.41248Quantitative Z-contrast Imaging in Scanning Transmission Electron Microscopy of Zeolite-supported Metal Clusters and Single-metal-atom Complexes With Single-Atom Sensitivity. Microscopy and Microanalysis, 2014, 20, 148-149.0.41249Ex Situ and In Situ (S)TEM of Iron Oxide Nanoparticles Synthesized by Decomposition of an Organometallic Precursor. Microscopy and Microanalysis, 2015, 21, 965-966.0.41250Revealing the Working Active Sites of M1 phase for Ethane Oxidation. Microscopy and Microanalysis, 2016, 22, 790-791.0.41251Electron Microscopy, Machine Learning, and Molecular Dynamics. Microscopy and Microanalysis, 2016, 21, 905-906.0.41	244	Photocatalytic water splitting with nano-K 4 Nb 6 O 17. Proceedings of SPIE, 2010, , .	0.8	1
240Nanoporous Metal in Soft Templates. Microscopy and Microanalysis, 2014, 20, 1600-1601.0.41247Implementing in situ Experiments in Liquids in the (Scanning) Transmission Electron Microscope ((S)TEM) and Dynamic TEM (DTEM). Microscopy and Microanalysis, 2014, 20, 1648-1649.0.41248Quantitative Z-contrast Imaging in Scanning Transmission Electron Microscopy of Zeolite-supported Metal Clusters and Single-metal-atom Complexes With Single-Atom Sensitivity. Microscopy and Microanalysis, 2014, 20, 148-149.0.41249Ex Situ and In Situ (S)TEM of Iron Oxide Nanoparticles Synthesized by Decomposition of an Organometallic Precursor. Microscopy and Microanalysis, 2015, 21, 965-966.0.41250Revealing the Working Active Sites of M1 phase for Ethane Oxidation. Microscopy and Microanalysis, 2016, 22, 790-791.0.41251The Mechanisms for Preferential Attachment of Nanoparticles in Liquid Determined Using Liquid Cell Electron Microscopy, Machine Learning, and Molecular Dynamics. Microscopy and Microanalysis, 0.40.41	245	Complete Water Splitting with Multi-Component Catalysts: Proposed Mechanism of Charge Transport in NiOx Loaded SrTiO3 Photocatalyst for Complete Water Splitting. Springer Theses, 2014, , 53-66.	0.1	1
247((\$)TEM) and Dynamic TEM (DTEM). Microscopy and Microanalysis, 2014, 20, 1648-1649.0.41248Quantitative Z-contrast Imaging in Scanning Transmission Electron Microscopy of Zeolite-supported Metal Clusters and Single-metal-atom Complexes With Single-Atom Sensitivity. Microscopy and Microanalysis, 2014, 20, 148-149.0.41249Ex Situ and In Situ (S)TEM of Iron Oxide Nanoparticles Synthesized by Decomposition of an Organometallic Precursor. Microscopy and Microanalysis, 2015, 21, 965-966.0.41250Revealing the Working Active Sites of M1 phase for Ethane Oxidation. Microscopy and Microanalysis, 2016, 22, 790-791.0.41251The Mechanisms for Preferential Attachment of Nanoparticles in Liquid Determined Using Liquid Cell Electron Microscopy, Machine Learning, and Molecular Dynamics. Microscopy and Microanalysis, 0.40.41	246	In Situ Observation of Directed Nanoparticle Aggregation During the Synthesis of Ordered Nanoporous Metal in Soft Templates. Microscopy and Microanalysis, 2014, 20, 1600-1601.	0.4	1
248Metal Clusters and Single-metal-atom Complexes With Single-Atom Sensitivity. Microscopy and0.41249Ex Situ and In Situ (S)TEM of Iron Oxide Nanoparticles Synthesized by Decomposition of an Organometallic Precursor. Microscopy and Microanalysis, 2015, 21, 965-966.0.41250Revealing the Working Active Sites of M1 phase for Ethane Oxidation. Microscopy and Microanalysis, 2016, 22, 790-791.0.41251The Mechanisms for Preferential Attachment of Nanoparticles in Liquid Determined Using Liquid Cell Electron Microscopy, Machine Learning, and Molecular Dynamics. Microscopy and Microanalysis, 0.40.41	247	Implementing in situ Experiments in Liquids in the (Scanning) Transmission Electron Microscope ((S)TEM) and Dynamic TEM (DTEM). Microscopy and Microanalysis, 2014, 20, 1648-1649.	0.4	1
249 Organometallic Precursor. Microscopy and Microanalysis, 2015, 21, 965-966. 0.4 1 250 Revealing the Working Active Sites of M1 phase for Ethane Oxidation. Microscopy and Microanalysis, 2015, 22, 790-791. 0.4 1 251 The Mechanisms for Preferential Attachment of Nanoparticles in Liquid Determined Using Liquid Cell 0.4 1	248	Metal Clusters and Single-metal-atom Complexes With Single-Atom Sensitivity. Microscopy and	0.4	1
2016, 22, 790-791. The Mechanisms for Preferential Attachment of Nanoparticles in Liquid Determined Using Liquid Cell 251 Electron Microscopy, Machine Learning, and Molecular Dynamics. Microscopy and Microanalysis, 0.4 1	249	Ex Situ and In Situ (S)TEM of Iron Oxide Nanoparticles Synthesized by Decomposition of an Organometallic Precursor. Microscopy and Microanalysis, 2015, 21, 965-966.	0.4	1
251 Electron Microscopy, Machine Learning, and Molecular Dynamics. Microscopy and Microanalysis, 0.4 1	250		0.4	1
	251	Electron Microscopy, Machine Learning, and Molecular Dynamics. Microscopy and Microanalysis,	0.4	1

The Potential for Imaging Dynamic Processes in Liquids with High Temporal Resolution. , 0, , 456-475.

#	Article	IF	CITATIONS
253	Imaging Electrochemical Processes in Li Batteries by Operando STEM. Microscopy and Microanalysis, 2017, 23, 1970-1971.	0.4	1
254	Phase Imaging: A Compressive Sensing Approach. Microscopy and Microanalysis, 2017, 23, 94-95.	0.4	1
255	Controlling the Reaction Process in Operando STEM by Pixel Sub-Sampling. Microscopy and Microanalysis, 2017, 23, 98-99.	0.4	1
256	Compressive Classification for TEM-EELS. Microscopy and Microanalysis, 2017, 23, 108-109.	0.4	1
257	Less is More: Bigger Data from Compressive Measurements. Microscopy and Microanalysis, 2017, 23, 166-167.	0.4	1
258	Manipulation and Immobilization of Nanostructures for In-situ STEM. Microscopy and Microanalysis, 2017, 23, 942-943.	0.4	1
259	Quantitative Mapping of Nanoscale Chemical Dynamics in Subâ€Sampled Operando (S)TEM Images using Spatioâ€Temporal Analytics. ChemCatChem, 2018, 10, 3115-3120.	3.7	1
260	Direct Atomic Scale Characterization of Interfaces and Doping Layers in Field-Effect Transistors Microscopy and Microanalysis, 2000, 6, 140-141.	0.4	0
261	Atomic Scale Characterization of Oxygen-Deficient Ceramic Membranes by EELS and Z-Contrast Imaging. Microscopy and Microanalysis, 2000, 6, 118-119.	0.4	0
262	The Role of Non-Stoichiometry in the Electrical Activity of Grain Boundaries in SrTiO3. Microscopy and Microanalysis, 2000, 6, 184-185.	0.4	0
263	Low-loss Electron Energy-loss Spectroscopy of Single CdSe Quantum Dots. Microscopy and Microanalysis, 2004, 10, 842-843.	0.4	0
264	Developing an Atomic Scale Model of Tilt Grain Boundary Potentials in Perovskite Oxides Using Z-contrast Imaging and EELS. Microscopy and Microanalysis, 2004, 10, 268-269.	0.4	0
265	Atomic Scale Characterization of the Pt/TiO2; Interface. Microscopy and Microanalysis, 2004, 10, 452-453.	0.4	0
266	Si0.85Ge0.15 oxynitridation in wet-nitric oxide ambient. Microelectronic Engineering, 2005, 77, 242-249.	2.4	0
267	Three Dimensional Observation of Flux Pinning Centers in Dy-doped YBa2Cu3O7-x Coated Superconductors by STEM Tomography. Materials Research Society Symposia Proceedings, 2007, 1026, 1.	0.1	0
268	Growth kinetics of InP nanowires heteroepitaxially grown on a silicon surface. Proceedings of SPIE, 2007, , .	0.8	0
269	Rücktitelbild: Imaging Isolated Gold Atom Catalytic Sites in Zeolite NaY (Angew. Chem. 24/2012). Angewandte Chemie, 2012, 124, 6120-6120.	2.0	0
270	Back Cover: Imaging Isolated Gold Atom Catalytic Sites in Zeolite NaY (Angew. Chem. Int. Ed. 24/2012). Angewandte Chemie - International Edition, 2012, 51, 6016-6016.	13.8	0

#	Article	IF	CITATIONS
271	Foreword. Ultramicroscopy, 2013, 127, 1.	1.9	Ο
272	Ex-situ and In-situ Analysis of MoVTeNb Oxide by Aberration-Corrected Scanning Transmission Electron Microscopy. Microscopy and Microanalysis, 2014, 20, 108-109.	0.4	0
273	The Oxygen Evolution Reaction: Water Oxidation Photocatalysis—Photocatalytic Water Oxidation with Suspended alpha-Fe2O3 Particles—Effects of Nanoscaling. Springer Theses, 2014, , 27-37.	0.1	0
274	Direct Observation of Li2O2 Nucleation and Growth with In-Situ Liquid ec-(S)TEM. Microscopy and Microanalysis, 2014, 20, 1608-1609.	0.4	0
275	Direct Observation of Aggregative Nanoparticle Growth: Kinetic Modeling of the Size Distribution and Growth Rate. Microscopy and Microanalysis, 2014, 20, 1612-1613.	0.4	0
276	Direct Observation of Electrolyte Degradation Mechanisms in Li-Ion Batteries. Microscopy and Microanalysis, 2014, 20, 1624-1625.	0.4	0
277	Applications of Bicrystallography: Revealing Generic Similarities in Coincidence Site Lattice Boundaries of all Holohedral Cubic Materials and Facilitating the Design of 3D Printed Models of such Grain Boundaries. Microscopy and Microanalysis, 2015, 21, 1453-1454.	0.4	0
278	Dose-rate controlled energy dispersive x-ray spectroscopic mapping of the metallic components in a biohybrid nanosystem. Semiconductor Science and Technology, 2016, 31, 084002.	2.0	0
279	Reliable Event Detection for Incomplete and Streaming (S)TEM Images. Microscopy and Microanalysis, 2017, 23, 158-159.	0.4	0
280	Quantifying Feature Uncertainty in Sub-sampled Low-dose (S)TEM Images. Microscopy and Microanalysis, 2017, 23, 160-161.	0.4	0
281	Resolution Versus Error for Computational Electron Microscopy. Microscopy and Microanalysis, 2017, 23, 88-89.	0.4	0
282	Digital Super-Resolution in EELS. Microscopy and Microanalysis, 2017, 23, 146-147.	0.4	0
283	Probing Dynamic Phase Transformations of Hydrated Iron Oxide Nanoparticles within situScanning Transmission Electron Microscopy. Microscopy and Microanalysis, 2017, 23, 858-859.	0.4	0
284	Cryo-STEM Tomography with Inpainting. Microscopy and Microanalysis, 2017, 23, 806-807.	0.4	0
285	ASCI: providing a forum for imaging scientists. Advanced Structural and Chemical Imaging, 2018, 4, 4.	4.0	0
286	Making Compressive Sensing Accessible in Scientific Imaging. Microscopy and Microanalysis, 2019, 25, 1684-1685.	0.4	0
287	Overall Photocatalytic Water Splitting with Suspended NiO-SrTiO3 Nanocrystals. Springer Theses, 2014, , 39-51.	0.1	0
288	The Complex Role of Aluminium Contamination in Nickelâ€Rich Layered Oxide Cathodes for Lithiumâ€Ion Batteries. Batteries and Supercaps, 2021, 4, 1783-1784.	4.7	0